IEEE Access
Multidisciplinary | Rapid Review | Open Access Journal

Received May 25, 2020, accepted May 30, 2020, date of publication June 8, 2020, date of current version June 18, 2020.

Digital Object Identifier 10.1109/ACCESS.2020.3000856

An Effective Stator Fault Diagnosis Framework of BLDC Motor Based on Vibration and Current Signals

TANVIR ALAM SHIFAT, (Graduate Student Member, IEEE), AND JANG WOOK HUR
Department of Mechanical Engineering, Kumoh National Institute of Technology, Gumi 39177, South Korea

Corresponding author: Jang Wook Hur (hhjw88@kumoh.ac.kr)

This work was supported by the National Research Foundation of Korea (NRF) funded by the Ministry of Science and ICT (MSIT), Korea Government under Grant 2019R1/1A3A01063935.

ABSTRACT Electric motor is a prominent rotary machinery in many engineering applications due to its excellent electrical energy utilization. With the increased demand in production and complex operating conditions, motors often run in a severe loading condition. Overload, overheating and many other intricate operating conditions account for the stator related faults in motors. Motor current signature analysis (MCSA) and vibration analysis have been popular techniques to diagnose different stator and rotor related faults in motors. But it is difficult to find the fault magnitude or fault threshold by using only one approach due to nonstationary motor operations. This paper presents a comprehensive review of a permanent magnet brushless DC motor's (BLDC motor) fault diagnosis combining vibration and current signals collected from sensors. Since the insulation break in the stator winding is the most commonly occurring fault in the stator, a short-circuit was artificially created between two windings. Based on the motor operating conditions, three health states are chosen from the experimental sensor data with different fault magnitudes. Health states are labeled as healthy state, incipient failure state, and severe failure state. Two effective fault diagnosis indices named kurtosis and third harmonic of motor current are selected for analyzing the vibration signals and current signals, respectively. Proposed diagnostics framework is validated using experimental data and proven to detect the stator fault at the early stage as well as distinguish between different fault states. Monitoring both mechanical and electrical characteristics of BLDC motor provides a thorough understanding of fault magnitude and threshold in different health states.

INDEX TERMS BLDC motor, condition monitoring, fault diagnosis, MCSA, stator fault, vibration signals.

I. INTRODUCTION

Predictive maintenance (PdM) is considered as a pivotal factor in many engineering systems to prevent unexpected failure and maximize productivity. To ensure maximum reliability of a system, a PdM framework helps to make some decisions by inspecting the trend of historical data or using a physical model of the system. However, lack of proper mathematical modeling and the ease in sensing, storing and analyzing big data have made the data-driven predictive maintenance framework a primary choice in industries [1]. There are two major steps in PdM: the first one is fault detection and diagnosis (FDD), which is to ascertain the current state of the component and inspect the root cause of the failure. The second one is the prognosis, which is to learn the trend of failure and predict the future state of the component based on historical data [1], [2]. A reliable prognostics methodology of PdM strategy mostly depends on the accuracy of the historical diagnostic framework. Therefore, robust fault diagnosis is a fundamental concern for different electrical and mechanical devices starting from a tiny transistor to large AC machines [3].

A. MOTIVATION

The most recent development on electric motors has been the invention of brushless dc (BLDC) motor, which is essentially a permanent magnet synchronous machine. The major advantage of BLDC motor is that it does not require any mechanical

The associate editor coordinating the review of this manuscript and approving it for publication was Filbert Juwono.

commutator, unlike conventional DC motors. Despite having greater reliability, a BLDC motor can also fail due to manufacturing defects, overload, earth fault, demagnetization, electromagnetic interference, etc. [4]. Winding related faults are the most commonly occurring faults in the stator coils of BLDC motors. Primary causes for winding faults are excessive heat, loose insulation, aging due to operation, contaminations, etc. [4]. Detecting these irregularities in an early stage can not only prevent a catastrophic failure but also protect human and environmental properties. Several studies have been conducted on fault diagnosis and condition monitoring of BLDC motor's stator related faults. MCSA has been the most popular technique to diagnose stator faults in motors [5]. Motor current carries significant information about the precision of stator winding operation [6]. Many studies have shown that the faults in the winding can be diagnosed at the earliest possible time by analyzing the current signature [7], [8]. J. K. Park *et al.* proposed stator current frequency analysis and input impedance monitoring for inter-turn faults of BLDC motors [9], [10]. S. Rajagopalan *et al.* used Wigner-Vile Distribution of motor currents to detect rotor related faults in nonstationary conditions [11]. S. T. Lee *et al.* used the analysis of third harmonic components of motor current to detect stator-related faults [12]. O. Moseler *et al.* proposed a model-based parameter estimation method for online fault detection [13]. A detailed survey of BLDC motors faults can be found in [14].

On the other hand, vibration analysis for fault diagnosis has been a prominent tool for rotary machinery like motors [15], wind turbines [16], gearboxes [17], and bearings [18]. Several kinds of research have undergone using the features, indexes and characteristics obtained from vibration signals in the presence of different faults [15], [18]–[21]. Kurtosis is considered as one of the most effective diagnostic features among them. Spectral kurtosis (SK) is an improvement over time-domain kurtosis and it can handle both stationary and nonstationary signals and localize the fault frequencies [22]. SK can be compared to narrowband amplitude demodulation techniques in the field of fault diagnosis and it does not require any historical data or prior knowledge. These qualities have made SK quite popular for the fault detection and isolation of different rotary machinery faults. Several studies have undergone diagnosing rotary machinery faults by using spectral kurtosis. For example, J. Tian *et al.* detected motor bearing fault from SK-based feature extraction [23]. J. Antoni *et al.* proposed STFT-based calculation of SK to characterize non-stationary signals [24]. Later, he used negentropy of squared envelope spectrum to represent impulsiveness called the Infogram [25]. Y. Lei *et al.* proposed wavelet packet transformation-based SK computation for the fault diagnosis of rolling element bearings [26]. Later, A. Moshrefzadeh *et al.* came up with the Autogram, to find the optimal demodulation band even in presence of strong noise in rotary machinery [27]. All these methods have a strong theoretical background and performance are validated using several machinery data such as rolling element bearing, gearbox etc. However, a detailed study on the brushless DC motor's fault diagnosis using SK has not been reported till date despite having a useful cyclostationarity behavior. In literature, most of the studies on BLDC motor's fault diagnosis deal with single sensor data. In practice, a motor is used to serve different purposes with unique operational complexity and environmental influence. It is understood that a higher load will cause the motor to draw larger amount of current from source than usual. Motor speed and torque can also get affected under certain stress and load. And, vibration for a motor totally depends on the system where it is operating. Therefore, monitoring only one parameter will not be sufficient to draw a conclusion about the motor health state. Moreover, A same fault can exhibit unique type of characteristics for different operating conditions and all the parameters do not show similar deviation from normal behavior at the same time. This is why authors of this study are motivated to establish a well-defined fault diagnostic framework using multiple sensor data. The main contribution of this proposed approach is the detection of motor winding related faults at the earliest possible time and categorize different fault states using the current and vibration signals, respectively.

B. PROPOSED METHOD

In this study, we propose an optimal diagnostic framework by combining Fast Kurtogram (FK), Autogram, and MCSA to diagnose BLDC motor winding short-circuit fault. Motor's vibration response for entire lifecycle is recorded using a piezotronics accelerometer. We divide the motor health states into three parts. One is the healthy state, at the beginning of the tests where all parameters are kept at rated values as per the manufacturer. Next state is when the fault is introduced by shorting two windings of the motor. We name this state as incipient failure state. The last one is the near breakdown stage when motor's performance dropped significantly, and we call it a severe failure state. Several parameters are considered to find the health state thresholds such as- stator coil temperature, noise and vibration, efficiency, motor, output voltage, rotating speed etc. Vibration signals from each health state are analyzed using fast kurtogram and Autogram to inspect the fault frequency and its magnitude. At the same time, third harmonic of motor current is analyzed to detect the fault at primary stage. To obtain a thorough understanding of current harmonics, this study presents a short-time Fourier transform (STFT) of motor current. STFT provides a better representation of current harmonics where the frequency is expressed as a function of time. A combination of motor current and vibration analysis gives a strong diagnosis framework and the transitions between different health states are accurately categorized with the help of combined electrical and mechanical characteristics investigation.

The remaining part of this paper is organized as follows. Section II of this paper highlights the theoretical background of the methods used to diagnose motor faults. Experimental setup and winding fault used for this study are explained in section III. Section IV presents the result analysis, discussion

and effectiveness of proposed diagnostics framework. Conclusion and prospect of using this type of technique are discussed in later section V.

II. RELATED THEORIES

The motor is necessarily an ergodic dynamical system that shows similar vibration response averaged over a certain timestamp. Naturally, there is a marginal discrepancy between a healthy state and a faulty state, which can be identified by simple frequency domain analysis. However, during the transition of health states, such as the beginning stage of health degradation, vibration changes so abruptly that only a time or frequency domain analysis cannot provide sufficient information to estimate the health state of the system. To capture these abruptly changing characteristics, analyzing the cyclostationarity of motor vibration signals is important and spectral kurtosis is a proven method for finding the impulsiveness of rotary machinery [24].

A. SPECTRAL KURTOSIS

Kurtosis is a widely used term in the probability theory and statistics which measures the deviation of a random dataset from the Gaussian distribution [28]. In any engineering field where data tends to be normal, kurtosis plays an important role in the detection of non-Gaussianity of the data. In the field of engineering maintenance, kurtosis acts as an indicator of signal impulsiveness, especially for rotary machinery vibration response [29], [30]. Statistical measurement of kurtosis is expressed in eq (1):

$$kurtosis\,(x) = \frac{E\{(x-\mu)^4\}}{\sigma^4} - 3 \tag{1}$$

where, x, μ and σ are time series signal, mean of the signal and standard deviation of the signal, respectively. Spectral kurtosis is an addition to the statistical measures that can detect the non-Gaussian component of the signal as well as find their locations in the frequency domain. Introduced by R. F. Dwyer, initially it was proposed to be complemented to power spectral density (PSD), a function that provides the frequency composition of energy of a signal [31]. V. Capdevielle *et al.* improved the definition of SK for higher order statistics and defined it as the fourth order cumulant of the Fourier transform [32]. J. Antoni presented an elaborated study on SK and established a formal theory to identify non-Gaussian characteristics for both stationary and nonstationary signals [33].

B. FAST KURTOGRAM

Kurtogram is a useful tool for the representation of spectral kurtosis. It assumes that in the fault state, uneven transients are associated with an optimal frequency/frequency resolution that maximizes the kurtosis values. Computation and representation of spectral kurtosis for a nonstationary signal are quite complicated because it is inherently used for Gaussian and stationary signals. J. Antoni had some research on finding solutions to these problems and came out with a formal representation of SK based on fast kurtogram [33], [34]. He used Wold's theorem, which was initially proposed for the decomposition of linear time variant signals for a dynamic evolution approximation. According to this theorem, finite time variant signals, in our case the motor vibration signals, can be expressed as the sum of two time series, one deterministic and another stochastic. Wold's decomposition for a finite length vibration signal, x(n) can be expressed as

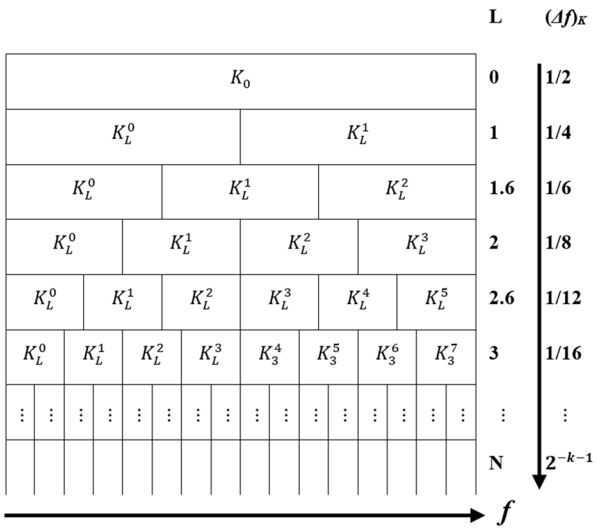

FIGURE 1. f/Δf plane representation for 1/3 binary tree Kurtogram estimation.

$$x\,(n) = \int_{-\frac{1}{2}}^{\frac{1}{2}} H(n,f)e^{j2\pi fn}dZ_x(f) \tag{2}$$

where, $dZ_x\,(f)$ is an orthonormal spectral increment and $H(n,f)$ is the complex envelope of x(n) at frequency f. Based on this envelope, SK can be expressed as

$$K_x\,(f) = \frac{\left\langle \left|H(n,f)^4\right| \right\rangle}{\left\langle \left|H(n,f)^2\right| \right\rangle^2} - 2 \tag{3}$$

The above equation holds several properties. The facts, that SK of a stationary process is proportional to frequency and SK of a stationary gaussian process is identically zero, will allow us to localize the presence of any additive sidebands in the signal. When there is a presence of fault in the vibration signal, some extraneous frequencies are found the spectrum. Kurtogram uses a ($\boldsymbol{f}$, $\boldsymbol{\Delta f}$) brace representation where f is the optimal frequency and $\boldsymbol{\Delta f}$ is frequency resolution which maximize the kurtosis. Figure 1 illustrates the ($\boldsymbol{f}$, $\boldsymbol{\Delta f}$) plane of kurtogram representation in 1/3 binary tree for N number of decomposition levels. Frequency localization and frequency concentration are two most important propositions of kurtogram to be implemented efficiently in practice. For the kurtogram to be interpreted as the kurtosis od the signal at a ($\boldsymbol{f}$, $\boldsymbol{\Delta f}$) pair, it should act like a band-pass filer i.e. ($\boldsymbol{f} - \boldsymbol{\Delta f}$; $\boldsymbol{f} + \boldsymbol{\Delta f}$). Also, to localize the frequency band to demodulate the signal, estimator should fulfill the Bedrossian's theorem

which implies $\Delta f \leq f$. To comply with these propositions, an effective 1/3 binary tree structure is used during the computation of Fast Kurtogram [33]. Major steps of FK computations are:

Step 1: Two prototype filters $h_0(n) = h(n)e^{j\pi n/4}$ and, $h_1(n) = h(n)e^{j3\pi n/4}$ are chosen to produce a tree of filter banks. This filter bank will generate a sequence of coefficients $c_k^i(n)$ from the i^{th} filter at the k^{th} level of decomposition. Here, i is the sequence number of filter and k is decomposition level number. It is worthy to mention that at $k = 0, c_0(n) = x(n)$.

Step 2: Later, high-pass sequences are transformed into low-pass sequences by taking a product of $(-j)^n$ after filtering with h_1 filter in order to preserve the frequency ordering.

Step 3: After a down sampling by a factor of 2, $c_k^i(n)$ produces two new sequences $c_{k+1}^{2i}(n)$ and $c_{k+1}^{2i+1}(n)$ at level k + 1.

Step 4: Step 2 is iterated from k = 0 to K − 1. At each level the number of filtered sequences is increased, and length is decreased by a factor of 2, so that the overall amount of datapoints remains the same.

Step 5: Computed coefficients $c_k^i(n)$ are interpreted as the complex envelope of signal x(n) as the frequency ordering is kept unchanged (Step 2). Then, the central frequency and the frequency resolution can be found as

$$f_i = \left(i + 2^{-1}\right) 2^{-k-1} \tag{4}$$

$$(\Delta f)_k = 2^{-k-1} \tag{5}$$

Step 6: The kurtogram is finally estimated by computing the kurtosis of all sequences $c_k^i(n)$ where, $i = 0, 1, 2 \ldots\ldots\ldots 2^k - 1$ and $k = 0, 1, 2, \ldots\ldots\ldots K - 1$ and can be expressed as follows:

$$K_k^i = \frac{\left\langle \left| c_k^i(n)^4 \right| \right\rangle}{\left\langle \left| c_k^i(n) \right|^2 \right\rangle^2} - 2 \tag{6}$$

C. AUTOGRAM

A. Moshrefzadeh et. al. proposed Autogram, based on unbiased autocorrelation (AC) to detect the transients even in presence of strong noise [25]. This method is already proven to be quite successful in detecting fault related information in bearings and gearboxes. Unlike using a filter-bank as mentioned in previous section, Autogram measures the kurtosis of complex envelope's unbiased autocovariance function making the best use of the cyclostationarity behavior [34]. There are mainly four steps of Autogram computations: briefly described below:

Step 1: Vibration signal is decomposed into frequency bands by means of wavelet transform. Unlike the filter-bank proposed in FK, Autogram uses Maximal Overlap Discrete Wavelet Packet Transform (MODWPT) for finding the optimal frequency bands. MODWPT is introduced to strengthen the WT coefficients that might get hampered due to down sampling. An elaborated description of MODWPT can be found in [35].

Step 2: The novelty of Autogram is that it uses autocovariance function to characterize 2nd order cyclostationarity of motor vibration signals. In this step, unbiased AC of squared envelope is computed for each node. AC has several advantages such as- it can remove uncorrelated components of the signal which are directly related to fault, also, since AC is performed in each node separately, SNR of the demodulated signal is increased. Instantaneous autocovariance function can be described as:

$$R_{xx}(t_i, \tau) = \boldsymbol{E}\{x(t_i - \tau/2)x(t_i + \tau/2)\} \tag{7}$$

$$R_{xx}(t_i, \tau) = R_{xx}(t_i + T, \tau) \tag{8}$$

here, $\tau = \frac{q}{Fs}; q = 0, 1, 2 \ldots\ldots\ldots N - 1$

$\mathbf{E}\{.\}$ is the expectation operator, x is the vibration signal, τ is the time lag and t_i is the instantaneous time.

Later, unbiased AC is computed as below:

$$\hat{R}_{XX}(\tau) = \frac{1}{N - q} \sum_{i=1}^{N-q} X(t_i)X(t_i + \tau) \tag{9}$$

X is the vibration signal filtered by MODWPT in Step 1.

Step 3: In this step, efficient frequency band for demodulation is selected for motor fault diagnosis. In kurtogram, it is done using the computed kurtosis from the filtered time signal. In Autogram, kurtosis values of all nodes resulting from step 2 is presented in a colormap. In this representation, color scale is proportional to kurtosis value, vertical axis presents the MODWPT decomposition level and horizontal axis presents the frequency. The modified equation of kurtosis, indicator of the impulsiveness of AC at each node, can be modified and expressed as

$$K_X = \frac{\sum_{i=1}^{N/2} \left[\hat{R}_{XX}(i) - \min(\hat{R}_{XX}(\tau))\right]^4}{\left[\sum_{i=1}^{N/2} \left[\hat{R}_{XX}(i) - \min(\hat{R}_{XX}(\tau))\right]^2\right]^2} \tag{10}$$

$$K_{X,u} = \frac{\sum_{i=1}^{N/2} \left|\hat{R}_{XX}(i) - \bar{X}_T(i)\right|_+^4}{\left[\sum_{i=1}^{N/2} \left|\hat{R}_{XX}(i) - \bar{X}_T(i)\right|_+^2\right]^2} \tag{11}$$

$$K_{X,l} = \frac{\sum_{i=1}^{N/2} \left|\hat{R}_{XX}(i) - \bar{X}_T(i)\right|_-^4}{\left[\sum_{i=1}^{N/2} \left|\hat{R}_{XX}(i) - \bar{X}_T(i)\right|_-^2\right]^2} \tag{12}$$

where N is the length of vibration signal. $|\blacksquare|_+$ and $|\blacksquare|_-$ mean that only positive and negative values are considered, respectively. $\bar{X}_T(i)$ is the threshold level and is defined as follows:

$$\bar{X}_T(i) = \frac{1}{k} \sum_{j=i}^{i+k-1} \hat{R}_{XX}(i) \tag{13}$$

Step 4: Lastly, fault characteristics frequencies are extracted for further diagnosis information from the signal.

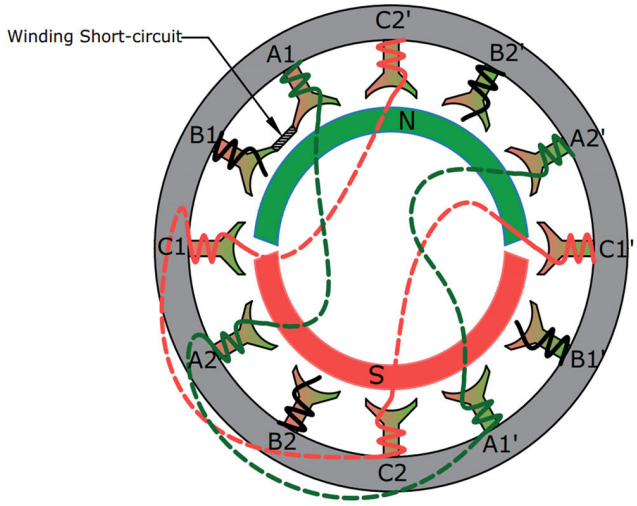

FIGURE 2. Winding distribution and fault location of BLDC motor used for testing.

The level and node where the impulsiveness takes place the most is also calculated as squared envelope spectrum (SES) [25], [35]. SES can be further extended to calculate other decomposition levels too to get an intuition about the strength of faulty level SES magnitude.

III. TEST BENCH AND DATA DESCRIPTION

Precise control, noiseless operation and reliability are the main advantages of BLDC motor. Since it lacks a mechanical commutator unlike conventional DC motors, commutation is done by electromagnetic induction between stator (electromagnets) and rotor (permanent magnet). The magnetic poles of stators are controlled by the current-carrying stator windings. When a coil is energized, it creates corresponding pole following the current polarity. And, the pole of stator electromagnet influences the nearest magnetic pole of rotor to rotate by continuous attraction and repulsion [36]. Since the BLDC motor's entire commutation is based on this electromagnetic property, a fault in the stator winding will largely affect the overall performance of BLDC motor. Winding short-circuit is one of the most commonly occurring faults in BLDC motors due to the insulation breakdown in high temperature or manufacturing defects.

There are many kinds of BLDC motors used for different purposes based on the kind of inputs, number of poles, rotor position, etc. The motor used for this study is a 2-pole interior permanent magnet (IPM) type of BLDC motor with 12 windings in the stator. An increased number of winding coils certainly gives better control and smooth operation of motor. Besides, this increases the chance of having a short-circuit among the windings due to manufacturing defects or aging caused by complex operations. In this experiment, we have created winding short-circuit deliberately by shorting two different windings. The illustration of BLDC motor's electrical commutation is presented in Fig. 2. The motor used for tests has 12 coil windings in the stator where 4 of them are interconnected to create a single phase. Thus, there are three combinations of phases each having four common windings connected together. Internally, these three phases are connected in a star connection with single common terminal and in the outer part, we have three terminals namely phase **A**, phase **B** and phase **C**. These phases are energized using an external input source with constant power supply. A motor driver is used to convert the DC input whose working principle is based on switching phenomena controlled by some transistors. Hall effect sensor (HES) is installed on each phase of the stator to know the exact location of rotor's poles, **N** and **S**. Based on the pole position, stator coils are excited with a positive current, negative current and no current at a certain time. This is done by the pulse width modulation (PWM) technique. For instance, in Fig. 2, phase **C** is excited with positive current and phase **A** is with negative current whereas phase **B** is not excited. For the next commutation step, phase **A** is negative, phase **B** is positive and phase **C** is kept disconnected. Rotary part, which is necessarily a permanent magnet, tries to align with the electromagnet's polarity but never catches it as the stator windings are energized with different polarity at a specific time interval, continuously.

Now, if there is a short-circuit between two adjacent windings, two different phases will be energized with same polarity at the same time. This will create a misalignment between the signal of HES and windings response. On the other hand, rotor will face interference on every rotation it makes leaving a series of impulses on motor's vibration. The magnitude of this impulsiveness is dependent on the speed of rotor and the number of windings having short-circuit. Several studies have shown the generation of noise and vibration due to imbalanced electromagnetic interference in permanent magnet motors [8], [37]. In practice, a variety of reasons cause this type of short-circuit staring from manufacturing defects to excessive heat in the stator coil due to complicated operating conditions. To investigate winding related faults, we created winding short-circuit fault by connecting A1 and B1 windings shown in Fig. 2 using a copper wire. This short-circuit caused excessive heat in initial stage and later gradual degradation of motor exhibiting irregular noise and vibration. Several motor parameters during the test were closely monitored such as motor currents, torque, speed, coil temperature, output voltage at the generator end etc. Threshold for different motor health states are obtained by analyzing the trend of changes in these parameters. For example, motor speed was dropped by a few hundred with time, but the noise and vibration produced by the motor increased significantly. A list of parameter thresholds can be found in Table 1.

To perform tests on BLDC motor, a conventional generator-motor (G-M) setup is used to avoid complexity and ease in collecting data different motor operating conditions. G-M setup allows us to build, control and modify motor external parameters to smoothly. Figure 3 represents the test bench photo where the tests were performed for the condition monitoring of the motor. The motor is controlled using a controller driver which has embedded hall effect sensors (HES) and

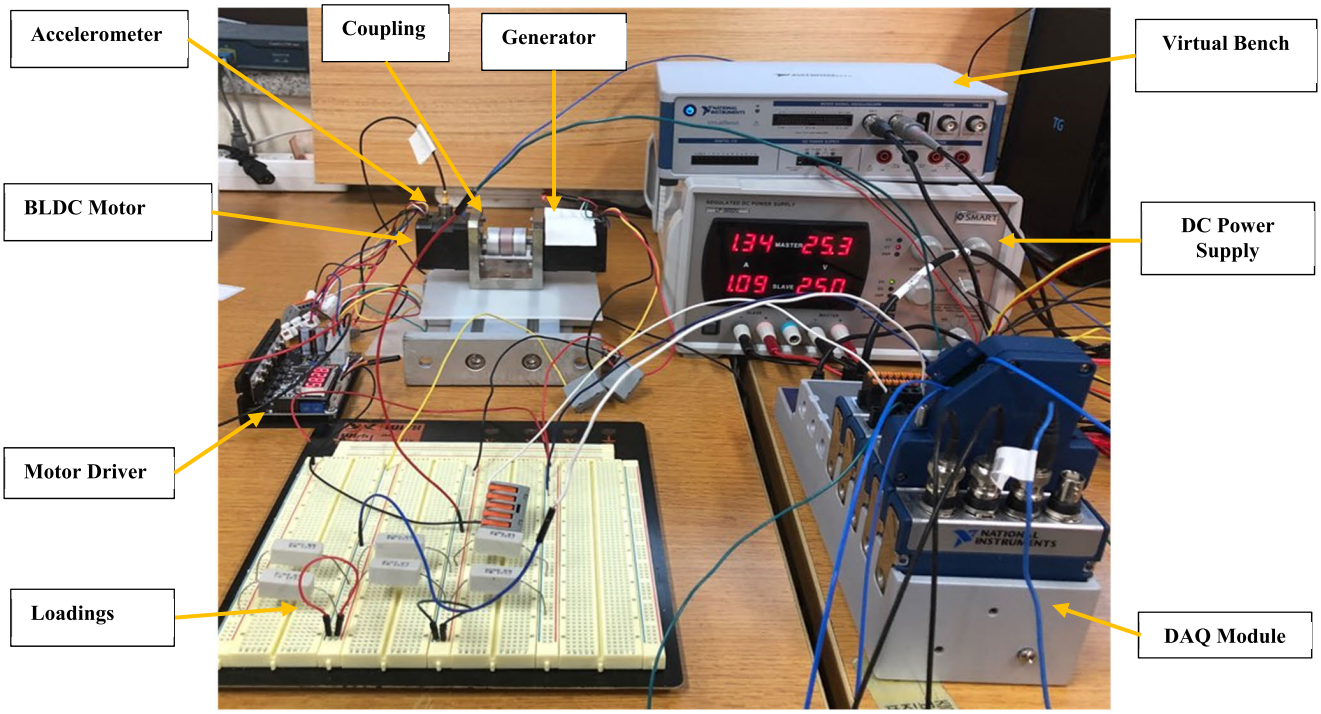

FIGURE 3. Test rig view of BLDC motor test.

TABLE 1. Thresholds for different health states.

Parameter	Threshold Value		
	Healthy	Incipient Failure	Severe Failure
Input voltage	DC 24V	DC 24V	DC 24V
Service time (Hours)	1-50	50-530	530-950
Motor speed (RPM)	3000	2630	2400
Line current (max)	2.6 A	4.5 A	4.5 A
Stator temperature	40-50 °C	115-130 °C	180-210 °C
Output voltage	11.3V±5%	9.5V±5%	5.5V±5%

TABLE 2. Parameters for motor test.

Parameter	Measurement
Motor Model	BLS-24026N
Generator Model	BLS-24040N
Accelerometer	PCB Piezotronics 352C04
DAQ Module [Vibration]	NI 9234
DAQ Module [Current]	NI 9246
Input	24 V_{DC} 7A (max)
Loads	10MΩ DELTA
Rated power	26W
Rated speed (No load)	4000 RPM
Sampling Rate (Vibration)	25.6 kHz
Sampling rate (Current)	5 kHz
Stator Coil Temperature	No Load: 40-60 °C

speed control potentiometer in it. 24 V_{DC} input was applied to the motor to power it up and some loads were connected with the generator in a delta configuration. Voltage produced at the generator indicates the efficiency of BLDC motor, which is also used as a parameter to categorize different health states. A brief description of major parameters for the motor test is shown in Table 2. During performing tests, vibration data was recorded using NI 9234 IEPE module and the sampling rate was set to be 25.6 kHz. Line currents were collected using NI 9246 module and sampled over 5 kHz frequency.

IV. RESULT ANALYSIS

A. FAULT DETECTION AND DIAGNOSIS

For this study, vibration response of the motor is monitored for the entire lifetime of motor and the data is represented in Fig. 4 for three different health states. Entire lifetime of the motor tested was around 450 hours. In the Fig. 4(a), only the stages where motor showed a transition from one health state to another are shown. Vibration was comparatively lower in healthy state compared to failure stages. Also, as the time goes, motor's vibration started to produce nonstationary signals with impulses. To closely speculate vibration signals, we took 10000 samples from each health states and the time series signal is presented in Fig. 4(b), 4(c)

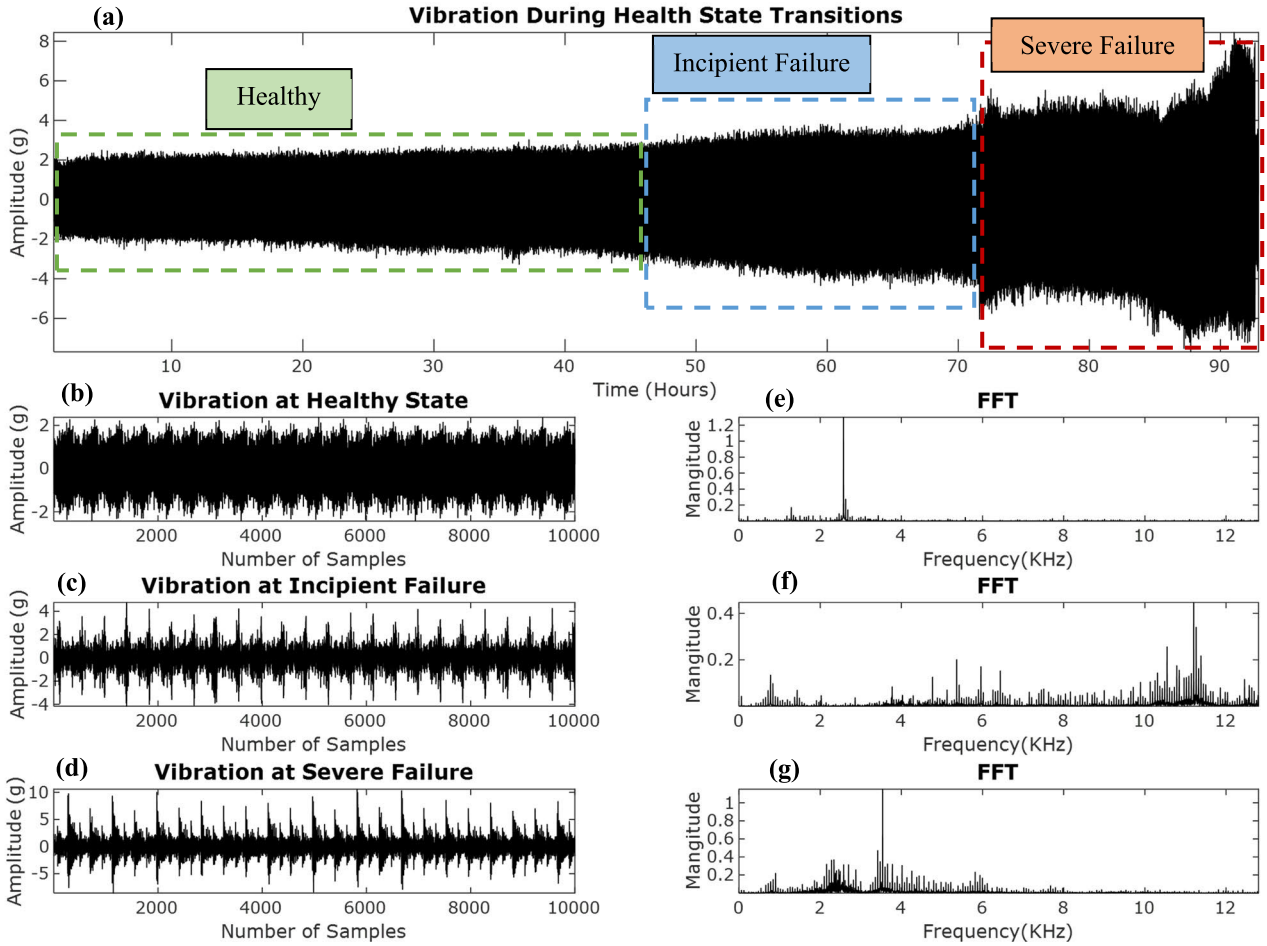

FIGURE 4. (a) Motor vibration response in different health states, (b) Healthy state vibration, (c) Incipient failure state vibration, (d) Severe failure state vibration, (e) Healthy state vibration in frequency domain, (f) Incipient failure state vibration at frequency domain, (g) Severe failure state in frequency domain.

and 4(d). Frequency domain representation is obtained by discrete Fourier transform (DFT) using a fast Fourier transform (FFT) algorithm. It can be noticed from Fig. 4(e)-4(g) that as the fault propagates, the presence of fault sidebands also increases as seen from the DFT transform of vibration signals in different states. FFT spectrums illustrated in Fig. 4 give us the intuition of the presence of fault frequencies in the signal. However, specifying the fault location and finding an optimum demodulation band is a challenging task just by observing the frequency domain representations. Therefore, a further efficient and adaptive technique; spectral kurtosis is used to represent the signals into different frequency levels.

Spectral kurtosis (SK) is proven to be highly efficient tool to detect impulsiveness in rotary machinery signals. However, in intricately varying circumstances, analyzing only the global kurtosis values might lead to an erroneous estimation. As seen from Figure 4(e)-4(g), there is a certain discrepancy between the frequency response of healthy state and faulty states. But, in terms of two faulty states, repetitive and fluctuating frequencies are making it difficult to come into a conclusion for a certain frequency range. This can be resolved by observing the signal's SK distribution in the frequency dyad. Finding the fault magnitude as a form of maximum spectral kurtosis will allow us to categorize different fault states. Therefore, we took the help of two different SK representation approaches of to find the most effective one.

For the fast kurtogram (FK) computation, we use the original sampling frequency 25.6 kHz which was used to acquire the vibration signals. Number of levels for frequency resolution was selected by a trial and error basis. After investigating different values, we choose 5 to balance the time-frequency resolution as well as a better fault identification. Figure 5 illustrates the FK representations of vibration signals separated by five levels in 1/3 binary tree. By analyzing these FK representations, we can easily determine the fault frequency, bandwidth, and frequency with the highest kurtosis etc. Figure 5(a) represents FK of motor vibration signal at healthy state with maximum kurtosis, $K_{max} = 0.9$ at level 1.6. Fig. 5(b) and 5(c) represent the FK for incipient and severe failure states with $K_{max} = 2.6$, and 5.7 at level 3.5 and 4, respectively. Center frequencies, f_c where the kurtosis is maximum is identified as 10.67 kHz, 11.20 kHz

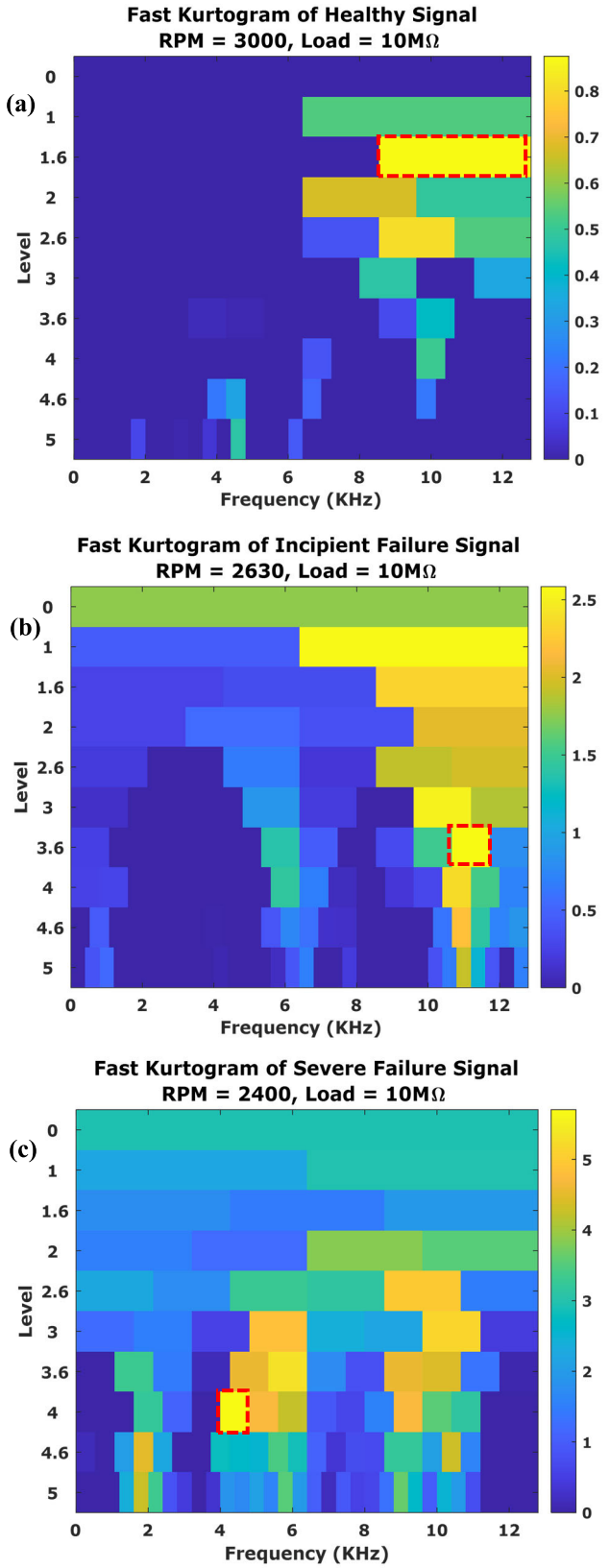

FIGURE 5. Vibration representations in Fast Kurtogram, (a) Healthy state, (b) Incipient failure state, (c) Severe failure state.

and 4.40 kHz for healthy, incipient failure and severe failure states, respectively. Bandwidth of K_{max} is also obtained from

TABLE 3. Features computed from fast kurtogram.

Feature	Measurement		
	Healthy	Incipient Failure	Severe Failure
Computation time (s)	8	9	8
K_{max}	0.9	2.6	5.7
Level	1.6	3.5	4
Bandwidth	4.70 kHz	1.67 kHz	800 Hz
Center Frequency, fc	10.67 kHz	11.2 kHz	4.4 kHz

FK analysis which indicated the range of frequency where the fault was stronger. Energy of the signal at the bandwidth carries significant information about the fault and can be considered as a diagnostics index too. On the Fig. 5(a), 5(b) and 5(c), bandwidth for maximum kurtosis is shown with red dotted lines for healthy, incipient failure and severe failure state, respectively. Summary of the diagnostic information extracted from FK computation is presented in Table 3.

On the other hand. Autogram computes the SK of vibration signals using a different type of filter named MODWPT as explained in section II. During computation, this filter is applied to vibration signals at each level of decomposition making it a slower process compared to FK computation. Moreover, computation becomes a bit more complex as the unbiased autocorrelation of the filtered signal is computed in this approach. As Autogram takes the measurements at each node separately with some complex estimations, it requires more computational time compared to FK. Autogram representation of vibration signals are shown in Fig. 6(a), 6(b) and 6(c) for healthy, incipient failure and severe failure states, respectively. Autogram shows brighter regions in colormap indicating maximum kurtosis values that are 5.8, 9.8 and 22.72 at level 5, 4 and 3 for healthy, incipient failure and severe failure states, respectively. The bandwidths computed by each technique is quite similar, but, the center frequency where the fault is localized, varies due to the different approach of computations. Maximum kurtosis calculated by Autogram is greater than that of FK approach for each health state signals. This implies Autogram will be robust technique for fault detection even in the presence of noise. Parameters measured from Autogram computation are presented in Table 4.

Analysis of spectral kurtosis for finding fault frequency and bandwidth provides significant information to distinguish between fault states with different fault magnitudes. Major advantage of SK compared to other non-stationary signal analysis techniques is that it can automatically indicate the demodulation frequency bandwidth without any prior knowledge. However, the initial degradation of health states and

TABLE 4. Features computed from Autogram.

Feature	Measurement		
	Healthy	Incipient Failure	Severe Failure
Computation time (s)	21	20	20
K_{max}	5.8	9.8	22.72
Level	5	4	3
Node	31	14	7
Bandwidth	400 Hz	800 Hz	1600 Hz
Center Frequency, f_C	11.8 kHz	10.8 kHz	10.4 kHz

the incipient failure moment cannot be detected effectively by this technique. Since a winding short-circuit was made in the stator winding of the motor, there was a significant change in phase current too.

Analyzing only the time series motor current is not sufficient to detect the variations in phase currents. Therefore, motor current is analyzed by determining frequency components using fast Fourier transform (FFT) and the density of frequency components using power spectral density (PSD). Fig. 7 represents the line current trends of BLDC motor in all three states of health. Time series current signals of all health states are presented in Fig. 7(a), 7(d) and 7(g). As the motor propagates to breakdown, it starts to draw more current from the source to keep the synchronous constant speed under similar loading and operating condition. Maximum current recorded for phase A is 2.6A at the healthy and incipient failure states whereas it increased to 4.5A at the severe failure state. Since the winding-short circuit was on phase A and phase B, both phases show identical characteristics throughout the entire lifecycle of motor operation. To avoid redundancy in fault characteristics, we present the current analysis of phase A only. The motor used for testing had a 120° conduction in a sex step continuous operation of phase A, phase B and phase C. Therefore, in a normal operation, tripled harmonics (3^{rd}, 6^{th}, 9^{th} . . .) which are necessarily zero sequence components, are not present in a phase current. This phenomenon follows the Kirchhoff's current law (KCL) which states the sum of three phase currents must be zero [7], [12]. Violation of KCL results a peak for every third harmonics of motor current spectra which can be observed from Fig. 7(b), 7(e) and 7(h). Third harmonic for healthy state current is not present whereas it has a noticeable peak for the faulty states. Power spectral density (PSD) gives a better intuition about the current characteristics by showing spectral energies as a function of frequency. Healthy state current signal has a lower signal strength compared to faulty states indicating distinguishable information. Maximum spectral

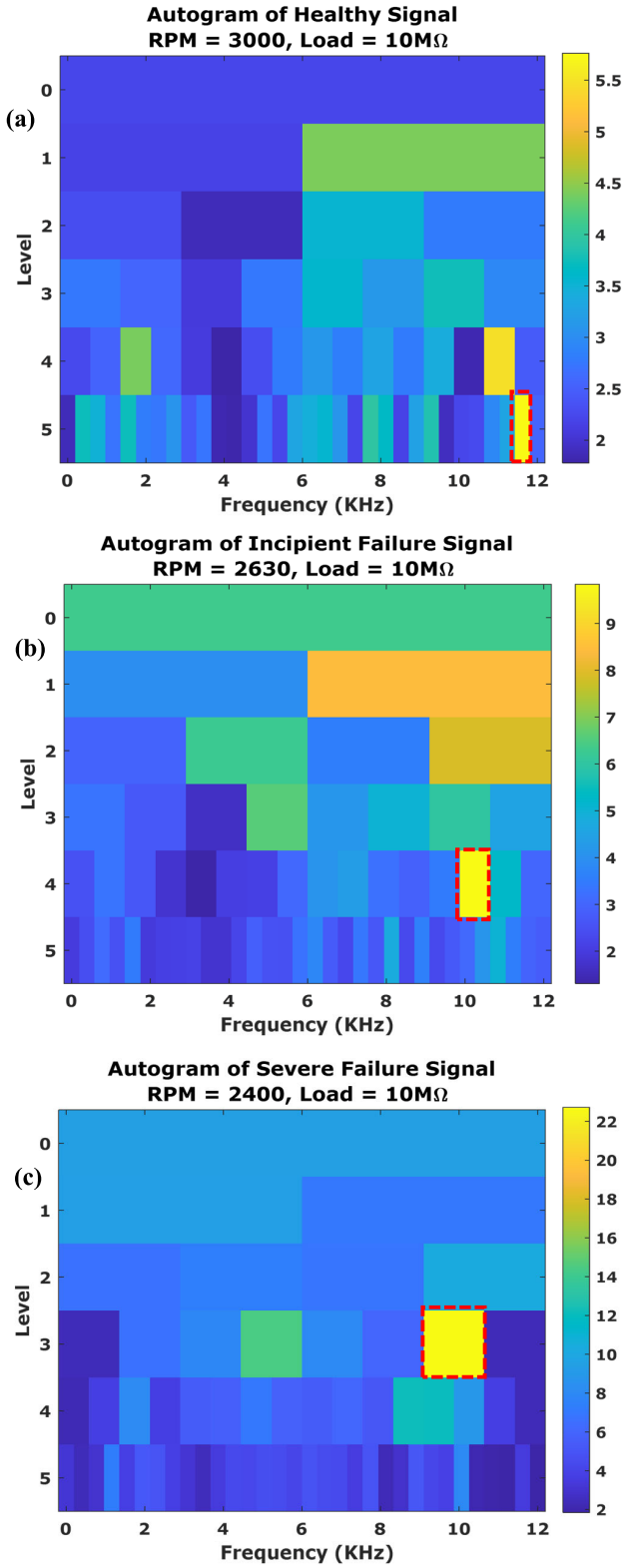

FIGURE 6. Vibration representations in Autogram. (a) Healthy state, (b) Incipient failure state, (c) Severe failure state.

energy recorded for healthy state current is -17 dB. On the other hand, -12 dB and -7 dB are recorded for incipient failure and severe failure states, respectively. However, PSD of motor

TABLE 5. Diagnostic information from MCSA.

Motor Current Parameter	Diagnostic Information					
	Healthy State		Incipient Failure		Severe Failure	
	F(Hz)	$\|I_A\|$	F(Hz)	$\|I_A\|$	F(Hz)	$\|I_A\|$
Fundamental frequency	241	1.50	237	1.49	225	1.45
3rd harmonic	-	-	918	0.25	1012	0.25
6th harmonic	-	-	1600	0.15	1790	0.12

current does not show variety of trends between incipient failure signal and severe failure signal making it not suitable for fault classification. Diagnostic features from MCSA are briefly presented in Table 5.

Since the FFT does not include the time domain information, we took the advantage of using short-time Fourier transform (STFT) to analyze current signals. In STFT, magnitude of frequency is presented as a function of time series samples acquired from sensor. Figure 8 is the STFT representation of motor current for different health states. The presence of third harmonic is clearly visible in the STFT spectrogram and the frequency magnitude of each harmonic is presented in a colormap format. 3rd and 6th harmonics of motor current are shown with red dashed rectangle in the STFT spectrogram presented in Fig. 8.

Besides localizing the impulsiveness in the vibration signal, the envelope responsible for the highest kurtosis, named squared envelope spectrum (SES) can also be extracted using these techniques. SES is commutated by taking FFT of the envelopes at the node with highest kurtosis using both demodulation approaches. Figure 9 represents the SES of different vibration signals extracted using FK and Autogram. Figure 9(b) and 9(e) are the complex envelopes of incipient and severe failure signals extracted at level 3.5 and 4 from FK at frequency 11.2 kHz and 4.4 kHz, respectively.

SES computed from Autogram are represented in Fig. 9(c) and 9(f) for incipient failure signal and severe failure signal at frequency level 10.8 kHz and 10.4 kHz, respectively. These SES imply the strength of faults in each health states of motor. One thing is noticeable from Fig. 9 is that the SES calculated from Autogram has a significantly higher peaks compared to that of FK computation. Since these spectrums indicates diagnostic information in the demodulation band, using Autogram to classify faulty types and fault magnitudes will provide a better outcome over FK.

B. PERFORMACE ANALYSIS OF PROPOSED METHOD

As in the initial state vibration does not change significantly, motor current signature analysis is an effective approach to monitor motor performance. MCSA is the most effective and in many cases the only way to diagnose stator-related faults at the incipient stage. This is also highlighted at the MCSA presented for this study too. Third harmonic of motor current is used as a diagnostic parameter and it showed clearly distinguishable trend in healthy and incipient failure state. However, the fluctuation of motor current did not occur drastically as the fault propagates which makes it difficult to categorize different fault types. As seen from third harmonic analysis, magnitude and frequency of harmonic components remain almost same for incipient and severe failure states. On the other hand, vibration analysis by taking advantage of spectral kurtosis provided distinguishable characteristics in both fault states. Meaningful information was extracted from different fault states by comparing the magnitude of spectral kurtosis at different frequency levels. Fast kurtogram and Autogram have shown great performance in extracting and analyzing fault magnitude from motor vibration signals. Due to the implementation of MODWPT filter and autocorrelation techniques, Autogram computation is more time consuming compared to fast kurtogram computation. However, extraction of a better SES for the faulty node has made Autogram a more advantageous technique. Information carried by SES can be further implemented for characterizing signals with higher noise.

Table 6 summarizes the proposed diagnosis framework combining multiple sensor data and fault detection techniques. For early fault detection, analyzing the motor current has been the best approach. To know the magnitude of fault and the frequency band in fault signals, spectral kurtosis can be computed using FK and Autogram. If the data size is large, FK should be used to find the demodulation band with fault as it requires a lesser amount of time. However, for a smaller dataset or noise affected dataset, Autogram will be preferred over FK.

Fault in the stator is regarded as a crucial form of fault in motors because at the beginning it might not show any external sign of warning. Gradually, it turns into a root cause of excessive heat, imbalanced line currents, reduction in torque, unusual vibration, etc. In cases, a trivial insulation break in stator winding can lead to breakdown of the motor's entire operation. Not to mention, in industrial applications this can create a catastrophe causing serious damage to properties as well as humans. Being an electromechanical system, monitoring both the electrical and mechanical behaviors of motor at the same time will provide the best possible outcome for the condition monitoring of motors. As seen from the study MCSA is a handy tool in detecting third harmonics in motor currents at the earliest stage of stator faults. On the other hand, FK and Autogram are two robust approaches to find the demodulation frequency band with highest kurtosis making a

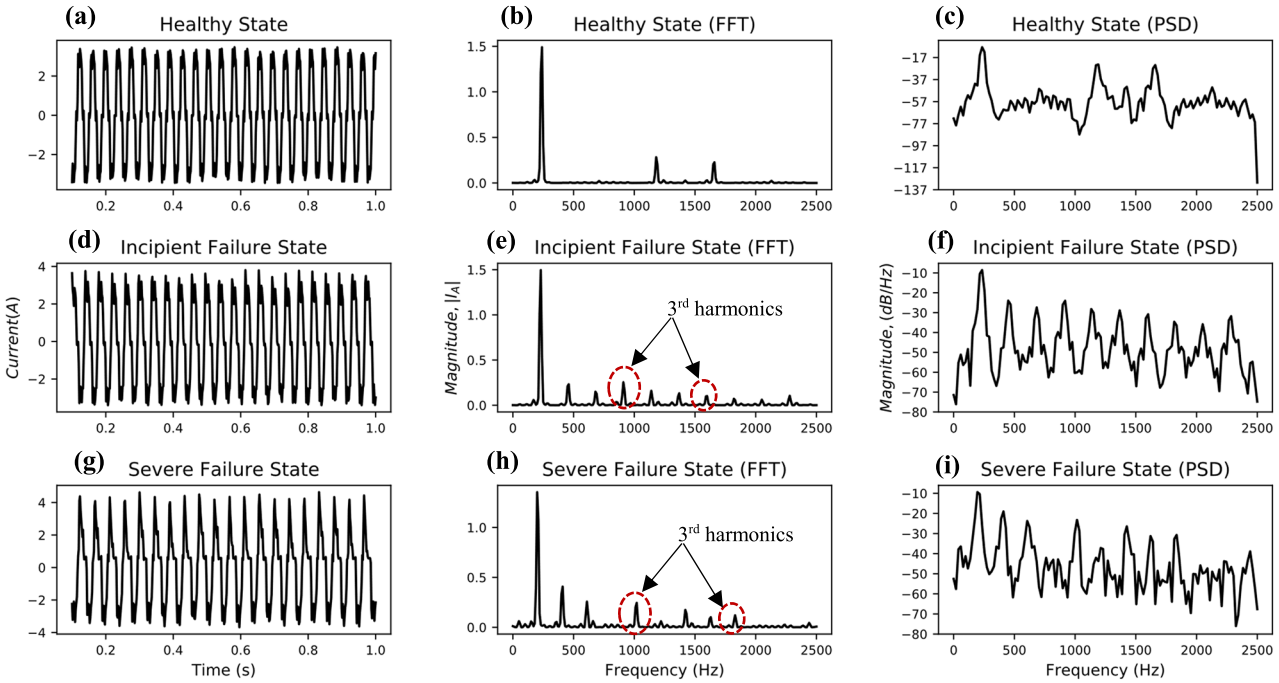

FIGURE 7. MCSA using FFT and PSD at different health states.

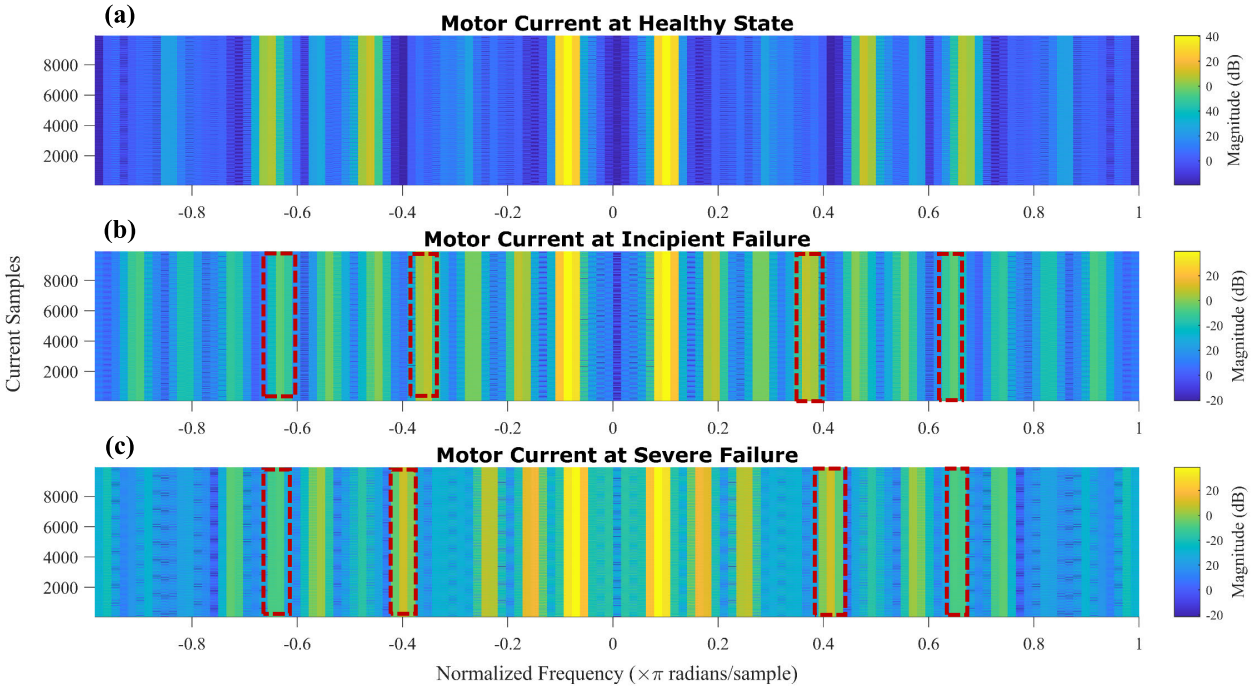

FIGURE 8. Time-frequency representation of motor current, (a) Healthy state, (b) Incipient failure state, (c) Severe failure state.

distinguishable fault patterns between incipient failure stage and severe failure stage.

Many other parameters can also be monitored for the FDD of motor such as- stator coil temperature, rotor bar magnetism, motor torque to name a few. But vibration and line current monitoring are quite simple techniques due to ease in data collection and comparatively cheaper measuring instruments. Moreover, vibration and current of a BLDC motor can be monitored continuously without interrupting the motor operation. This type of online condition monitoring will reduce the risk of system failure by detecting the faults at the earliest stage. Also, demodulation frequency and fault magnitudes extracted from vibration analysis can be further implemented for decision making and prognostics.

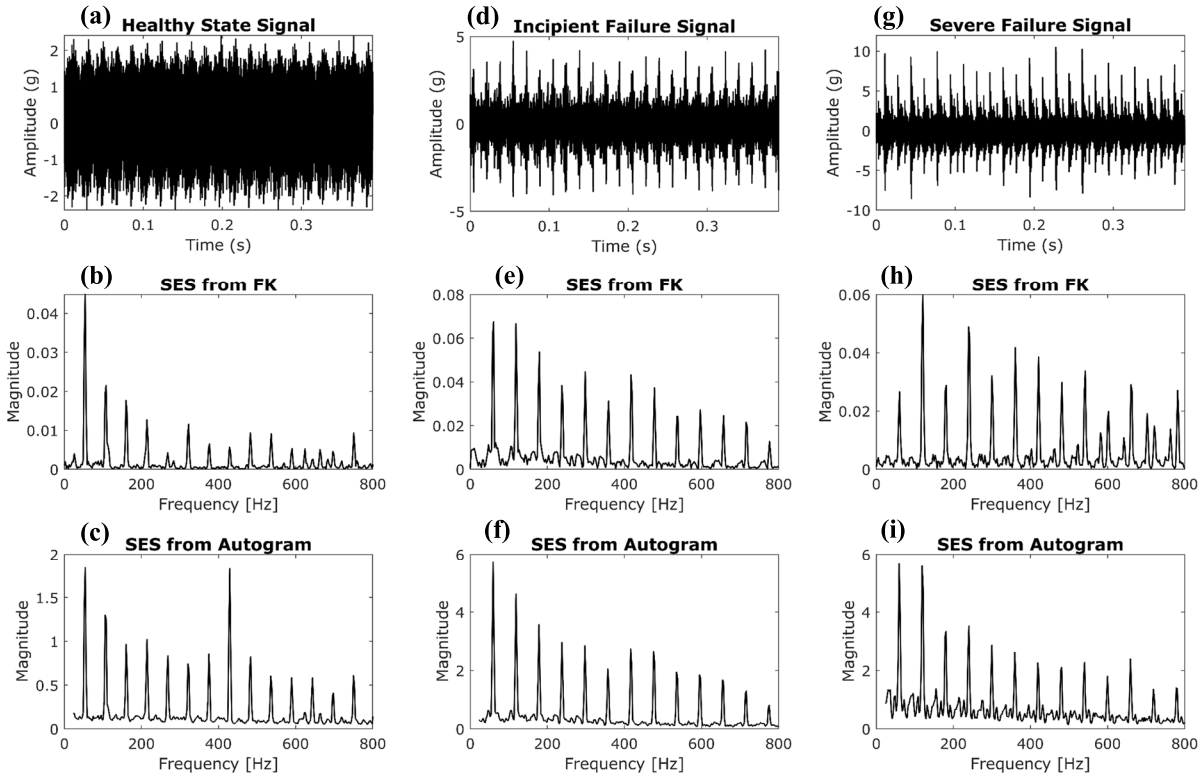

FIGURE 9. (a) Vibration signal at healthy state, (b) FK computation of SES at healthy state, (c) Autogram computation of SES at healthy state, (d) Vibration signal at incipient failure state, (e) FK computation of SES for the level with fault, (f) Autogram computation of SES for the level with fault, (g) Vibration signal at severe failure state, (h) FK computation of SES for the level with fault, (i) Autogram computation of SES for the level with fault.

TABLE 6. Summary of proposed diagnostics framework.

Method	Significance in terms of winding fault diagnosis
Fast Kurtogram	Not a reliable approach to estimate the healthy state of motor. It was able to accurately diagnose and locate fault frequencies and demodulation bandwidth. Also, it was able to distinguish between both fault states by SK computation. However, SES extracted using FK has a weak characteristic which is might be inefficient for the cases with noisy signals.
Autogram	This approach provided marginal discrepancy between incipient and severe failure states making it easier to categorize different faults. SES extracted using Autogram can be effectively applied to noise affected signals too. However, since the Autogram is based on the estimation of kurtosis at different nodes, it is not an effective approach to use in healthy state.
MCSA	Carries significant information about healthy state. Analysis of current signature as well as time series motor current characterizes the healthy state of motor. The presence of third harmonics provided sufficient information to diagnose fault at the earliest possible time.

V. CONCLUSION

This study reports the diagnosis and detection of winding short-circuit fault in a permanent magnet BLDC motor using multi-sensor data. A fault was deliberately created by shorting two windings of stator coil causing irregularity in the electromagnetic commutation. Due to this fault, initially excessive heat was produced at the stator coil and motor's normal operation declined gradually over time. To diagnose and categorize different health states, data acquired from multiple sensors such as- current and vibration are used. Monitoring both the electrical and mechanical behavior of BLDC motor at the same time provides a thorough and accurate condition monitoring in the presence of winding fault. Spectral kurtosis computed from vibration signals is considered as a diagnostic index as it carries significant information about the signal impulsiveness. Fast kurtogram and Autogram are used to compute and represent kurtosis at different frequency levels and their performance is evaluated based on different health states of motor. Both methods are found to be quite effective in detection and localization of transients and hidden

nonstationary. However, the early fault or the incipient failure moment is a difficult to detect by estimating the kurtosis values since the vibration will be varied in different operating conditions. So, we took the advantage of motor current signature analysis for early fault detection as it carries significant information about the irregularity in stator winding. Inspection of third harmonic of stator current provided distinctive evidence to categorize healthy and faulty states. Besides, analyzing the motor current in time-frequency domain gives a better intuition about the fault magnitude and instance at the earliest possible time. Monitoring and analyzing multi-sensor data have presented better intuition about the fault magnitude and threshold.

This work can be further extended to diagnosis of several other motor faults such as rotor bar related faults, eccentricity faults, demagnetization faults etc. Diagnostics information found from this study will further be implemented for the prognostics of BLDC motor which is a crucial part of predictive maintenance.

REFERENCES

[1] A. K. S. Jardine, D. Lin, and D. Banjevic, "A review on machinery diagnostics and prognostics implementing condition-based maintenance," *Mech. Syst. Signal Process.*, vol. 20, no. 7, pp. 1483–1510, Oct. 2006.
[2] R. Ahmad and S. Kamaruddin, "An overview of time-based and condition-based maintenance in industrial application," *Comput. Ind. Eng.*, vol. 63, no. 1, pp. 135–149, Aug. 2012.
[3] M. Pecht, and M. Kang, *Prognostics and Health Management of Electronics: Fundamentals, Machine Learning, and the Internet of Things*. Hoboken, NJ, USA: Wiley, Aug. 2018, pp. 1–8, doi: 10.1002/9781119515326.
[4] S. Nandi, H. A. Toliyat, and X. Li, "Condition monitoring and fault diagnosis of electrical motors—A review," *IEEE Trans. Energy Convers.*, vol. 20, no. 4, pp. 719–729, Dec. 2005.
[5] S. Kumar, D. Mukherjee, P. K. Guchhait, R. Banerjee, A. K. Srivastava, D. N. Vishwakarma, and R. K. Saket, "A comprehensive review of condition based prognostic maintenance (CBPM) for induction motor," *IEEE Access*, vol. 7, pp. 90690–90704, 2019.
[6] C. Kar and A. R. Mohanty, "Monitoring gear vibrations through motor current signature analysis and wavelet transform," *Mech. Syst. Signal Process.*, vol. 20, no. 1, pp. 158–187, Jan. 2006.
[7] S. Nandi, "Detection of stator faults in induction machines using residual saturation harmonics," *IEEE Trans. Ind. Appl.*, vol. 42, no. 5, pp. 1201–1208, Sep. 2006.
[8] Y. Da, X. Shi, and M. Krishnamurthy, "A new approach to fault diagnostics for permanent magnet synchronous machines using electromagnetic signature analysis," *IEEE Trans. Power Electron.*, vol. 28, no. 8, pp. 4104–4112, Aug. 2013.
[9] J.-K. Park and J. Hur, "Detection of inter-turn and dynamic eccentricity faults using stator current frequency pattern in IPM-type BLDC motors," *IEEE Trans. Ind. Electron.*, vol. 63, no. 3, pp. 1771–1780, Mar. 2016.
[10] J.-K. Park, C.-L. Jeong, S.-T. Lee, and J. Hur, "Early detection technique for stator winding inter-turn fault in BLDC motor using input impedance," *IEEE Trans. Ind. Appl.*, vol. 51, no. 1, pp. 240–247, Jan. 2015.
[11] S. Rajagopalan, J. M. Aller, J. A. Restrepo, T. G. Habetler, and R. G. Harley, "Detection of rotor faults in brushless DC motors operating under nonstationary conditions," *IEEE Trans. Ind. Appl.*, vol. 42, no. 6, pp. 1464–1477, Nov. 2006.
[12] S.-T. Lee and J. Hur, "Detection technique for stator inter-turn faults in BLDC motors based on third-harmonic components of line currents," *IEEE Trans. Ind. Appl.*, vol. 53, no. 1, pp. 143–150, Jan. 2017.
[13] O. Moseler and R. Isermann, "Application of model-based fault detection to a brushless DC motor," *IEEE Trans. Ind. Electron.*, vol. 47, no. 5, pp. 1015–1020, Oct. 2000.
[14] Y. Da, X. Shi, and M. Krishnamurthy, "Health monitoring, fault diagnosis and failure prognosis techniques for brushless permanent magnet machines," in *Proc. IEEE Vehicle Power Propuls. Conf.*, Sep. 2011, pp. 1–7.
[15] D. Wang, K.-L. Tsui, and Q. Miao, "Prognostics and health management: A review of vibration based bearing and gear health indicators," *IEEE Access*, vol. 6, pp. 665–676, 2018.
[16] W. Yang, P. J. Tavner, C. J. Crabtree, Y. Feng, and Y. Qiu, "Wind turbine condition monitoring: Technical and commercial challenges," *Wind Energy*, vol. 17, no. 5, pp. 673–693, May 2014.
[17] Y. Lei, J. Lin, M. J. Zuo, and Z. He, "Condition monitoring and fault diagnosis of planetary gearboxes: A review," *Measurement*, vol. 48, pp. 292–305, Feb. 2014.
[18] R. Yan, R. X. Gao, and X. Chen, "Wavelets for fault diagnosis of rotary machines: A review with applications," *Signal Process.*, vol. 96, pp. 1–15, Mar. 2014.
[19] N. Su, X. Li, and Q. Zhang, "Fault diagnosis of rotating machinery based on wavelet domain denoising and metric distance," *IEEE Access*, vol. 7, pp. 73262–73270, 2019.
[20] R. B. Randall, *Vibration-Based Condition Monitoring: Industrial, Aerospace and Automotive Applications*. Hoboken, NJ, USA: Wiley, 2011.
[21] P. S. Addison, *The Illustrated Wavelet Transform Handbook: Introductory Theory and Applications in Science, Engineering, Medicine and Finance*. Boca Raton, FL, USA: CRC Press, 2017.
[22] Y. Wang, J. Xiang, R. Markert, and M. Liang, "Spectral kurtosis for fault detection, diagnosis and prognostics of rotating machines: A review with applications," *Mech. Syst. Signal Process.*, vols. 66–67, pp. 679–698, Jan. 2016.
[23] J. Tian, C. Morillo, M. H. Azarian, and M. Pecht, "Motor bearing fault detection using spectral kurtosis-based feature extraction coupled with K-Nearest neighbor distance analysis," *IEEE Trans. Ind. Electron.*, vol. 63, no. 3, pp. 1793–1803, Mar. 2016.
[24] J. Antoni, "The spectral kurtosis: A useful tool for characterising non-stationary signals," *Mech. Syst. Signal Process.*, vol. 20, no. 2, pp. 282–307, Feb. 2006.
[25] J. Antoni, "The infogram: Entropic evidence of the signature of repetitive transients," *Mech. Syst. Signal Process.*, vol. 74, pp. 73–94, Jun. 2016.
[26] Y. Lei, J. Lin, Z. He, and Y. Zi, "Application of an improved kurtogram method for fault diagnosis of rolling element bearings," *Mech. Syst. Signal Process.*, vol. 25, no. 5, pp. 1738–1749, Jul. 2011.
[27] A. Moshrefzadeh and A. Fasana, "The autogram: An effective approach for selecting the optimal demodulation band in rolling element bearings diagnosis," *Mech. Syst. Signal Process.*, vol. 105, pp. 294–318, May 2018.
[28] H. Zhang, X. Chen, Z. Du, and R. Yan, "Kurtosis based weighted sparse model with convex optimization technique for bearing fault diagnosis," *Mech. Syst. Signal Process.*, vol. 80, pp. 349–376, Dec. 2016.
[29] G. L. McDonald, Q. Zhao, and M. J. Zuo, "Maximum correlated kurtosis deconvolution and application on gear tooth chip fault detection," *Mech. Syst. Signal Process.*, vol. 33, pp. 237–255, Nov. 2012.
[30] S. Liu, S. Hou, K. He, and W. Yang, "L-kurtosis and its application for fault detection of rolling element bearings," *Measurement*, vol. 116, pp. 523–532, Feb. 2018.
[31] R. Dwyer, "Detection of non-Gaussian signals by frequency domain kurtosis estimation," in *Proc. IEEE Int. Conf. Acoust., Speech, Signal Process. (ICASSP)*, vol. 8, Apr. 1983, pp. 607–610.
[32] V. Capdevielle, C. Serviere, J.-L. Lacoume, "Blind separation of wide-band sources: Application to rotating machine signals," in *Proc. 8th Eur. Signal Process. Conf. (EUSIPCO)*, 1996, pp. 1–4.
[33] J. Antoni and R. B. Randall, "The spectral kurtosis: Application to the vibratory surveillance and diagnostics of rotating machines," *Mech. Syst. Signal Process.*, vol. 20, no. 2, pp. 308–331, Feb. 2006.
[34] J. Antoni, "Fast computation of the kurtogram for the detection of transient faults," *Mech. Syst. Signal Process.*, vol. 21, no. 1, pp. 108–124, Jan. 2007.
[35] A. Moshrefzadeh, A. Fasana, and L. Garibaldi, "Analysis of autogram performance for rolling element bearing diagnosis by using different data sets," in *Proc. Int. Conf. Condition Monit. Machinery Non-Stationary Oper.* Cham, Switzerland: Springer, 2018, pp. 132–141.
[36] S.-H. Kim, *Electric Motor Control: DC, AC, and BLDC Motors*. Amsterdam, The Netherlands: Elsevier, 2017, pp. 389–416.
[37] H.-S. Ko and K.-J. Kim, "Characterization of noise and vibration sources in interior permanent-magnet brushless DC motors," *IEEE Trans. Magn.*, vol. 40, no. 6, pp. 3482–3489, Nov. 2004, doi: 10.1109/TMAG.2004.832991.

TANVIR ALAM SHIFAT (Graduate Student Member, IEEE) received the B.Sc. degree in electrical and electronic engineering from East West University, Bangladesh, in 2016. He is currently a Graduate Student at the Department of Mechanical System Engineering, Kumoh National Institute of Technology. He is also working as a full-time Graduate Research Assistance at the Defense Reliability and Maintainability Research Laboratory. He is primarily focused on the advanced signal processing and machine learning techniques for the condition monitoring of electric motors. His research interests include reliability, maintainability, condition monitoring of rotary machinery, and electronic devices.

JANG WOOK HUR received the Ph.D. degree in mechanical engineering from Tokyo Institute of Technology, Japan, in 1995. He is currently serving as a Professor at the Department of Mechanical Engineering, Kumoh National Institute of Technology, where he is the Director of the Defense Reliability and Maintainability Research Laboratory. He also served for Korean Army, and ranked Colonel, in 2011. His research interests include reliability, maintainability, and condition monitoring of various defense equipment.